Pharm Res (2014) 31:2664–2676
DOI 10.1007/s11095-014-1363-x

RESEARCH PAPER

Quantiosomes as a Multimodal Nanocarrier for Integrating Bioimaging and Carboplatin Delivery

Chwan-Fwu Lin • Chih-Jen Wen • Ibrahim A. Aljuffali • Chun-Lin Huang • Jia-You Fang

Received: 8 November 2013 / Accepted: 15 March 2014 / Published online: 7 June 2014

ABSTRACT

Purpose Here we report the development of quantiosomes, niosomes formed from Span 60, cholesterol, and quantum dots (QDs), for achieving sensitive bioimaging and anticancer drug delivery.

Methods The nanocarriers were further modified by incorporating soy phosphatidylcholine (SPC), polyethylene glycol (PEG), or cationic surfactant to display different efficiencies. Carboplatin was used as the model drug. The cellular uptake, cytotoxicity, and migration inhibition of quantiosomes for treating melanoma cells were described. Finally, intratumoral carboplatin accumulation and *in-vivo* bioimaging were examined.

Results The average diameters of quantiosomes ranged between 151 and 173 nm, depending on the composition selected. Approximately 50% of the drug was entrapped in quantiosomes. Electron microscopy confirmed the bilayer structure of quantiosomes and the presence of QDs in the vesicular surface. The nanodispersions showed a significant internalization into cells, especially the cationic formulations. Quantiosomes increased cytotoxicity against melanoma by 3～4-fold as compared to free carboplatin. *In-vivo* intratumoral administration demonstrated an increased drug depot in melanoma from 6 to 10 ng/mg by SPC-loaded and PEGylated quantiosomes relative to aqueous control. *In-vivo* fluorescence imaging showed that quantiosomes reduced leakage of QDs from melanoma. A fluorescence signal confined in tumors could be sustained for at least 24 h. Quantiosomes also exhibited a sensitive and prolonged fluorescence in ovarian tumors.

Conclusion Niosomes containing QDs and carboplatin as a multifunctional nanosystems provide a non-expensive and efficient strategy to prolong drug retention and fluorescence signal in tumors.

KEY WORDS Bioimaging · Melanoma · Niosomes · Quantiosomes · Quantum dots

Electronic supplementary material The online version of this article (doi:10.1007/s11095-014-1363-x) contains supplementary material, which is available to authorized users.

C.-F. Lin
Department of Cosmetic Science, Chang Gung University of Science and Technology, Kweishan, Taoyuan, Taiwan

C.-F. Lin
Chronic Diseases and Health Promotion Research Center, Chang Gung University of Science and Technology, Kweishan, Taoyuan, Taiwan

C.-J. Wen
School of Medicine, Chang Gung University, Kweishan, Taoyuan, Taiwan

C.-J. Wen
Center for Vascularized Composite Allotransplantation, Chang Gung Memorial Hospital, Kweishan, Taoyuan, Taiwan

I. A. Aljuffali
Department of Pharmaceutics, College of Pharmacy, King Saud University, Riyadh, Saudi Arabia

C.-L. Huang • J.-Y. Fang (✉)
Pharmaceutics Laboratory, Graduate Institute of Natural Products Chang Gung University, 259 Wen-Hwa 1st Road, Kweishan, Taoyuan 333, Taiwan
e-mail: fajy@mail.cgu.edu.tw

J.-Y. Fang
Chinese Herbal Medicine Research Team, Healthy Aging Research Center, Chang Gung University, Kweishan, Taoyuan, Taiwan

J.-Y. Fang
Research Center for Industry of Human Ecology, Chang Gung University of Science and Technology, Kweishan, Taoyuan, Taiwan

INTRODUCTION

Quantum dots (QDs) are semiconductor nanocrystals, which can be employed to be fluorescent probes because of their fluorescence intensity, tunable spectra, and greater photostability than organic dyes (1). However, the applicability of QDs in biology and medicine is limited due to concern about their toxicity and the difficulty they have penetrating cells or endocytic compartments (2). One strategy to resolve this problem is to load QDs in liposomes for imaging purposes. Liposomes are a nanoscale structure composed of phospholipid bilayers surrounding a water core. Entrapment of QDs in liposomes provides benefits of enhanced biocompatibility, fluorescence stability, and stable dispersion in biological fluids (3). There are some reports investigating the effect of liposomes for improving bioimaging of QDs (4–6). Some drawbacks restrict clinical use of liposomes. These include difficulty with sterilization, trouble with large-scale preparation, instability in storage and biosystems, as well as high cost (7). Hence, a novel alternative is needed to replace liposomes for QD encapsulation.

Niosomes are non-ionic surfactant vesicles with lamellar bilayers produced from non-ionic surfactants and cholesterol, offering a substitute for liposomes (8). Niosomes provide advantages over liposomes such as high stability, ease of preparation, high purity, and low cost (9,10). These positive features lead to attractive applications of niosomes for industry and clinics. Niosomes have been extensively used as nanocarriers for delivering anticancer drugs. Multifunctional nanomedicine is a novel generation of medicine that integrates bioimaging, drug targeting, and therapy for synchronous diagnosis and drug treatment (11). The prime objective of this work was to formulate QDs and anticancer drugs into niosomes and to assess delivery ability and bioimaging for melanoma. Here, we introduced "quantiosomes" for achieving this aim, which was a niosomal system containing carboxyl QDs. Melanoma is usually misdiagnosed due to its resemblance to blood blisters, hemangiomas, and dermal nevi (12). Moreover, melanoma is highly resistant to regular chemotherapy, resulting in poor prognosis (13). The achievement of early diagnosis and efficient therapy is urgently needed. Carboplatin was used as the drug to be encapsulated by quantiosomes in this report. It is an alternative to cisplatin for treating metastatic melanoma with equal efficacy and fewer adverse effects (14).

The present work reported the preparation, physicochemical properties, cell uptake, antitumor potential, intratumoral drug concentration, and *in-vivo* bioimaging of the developed quantiosomes. The vesicle size, surface charge, morphology, and carboplatin entrapment were characterized. *In-vitro* experiments on cellular uptake, cytotoxicity, and migration inhibition against melanoma were performed. *In-vivo* accumulation of carboplatin in melanoma and real-time imaging of quantiosomes were evaluated after intratumoral administration. In addition to melanoma cells, ovarian cancer cells were used for comparison. In the present study, we have developed niosomal systems combining QDs and drugs as a multimodal nanocarrier.

MATERIALS AND METHODS

Materials

Carboplatin, Span 60, cholesterol, and Nile red were purchased from Sigma-Aldrich (St. Louis, MO, USA). Hydrogenated soy phosphatidylcholine (SPC, Phospholipon 80H®) was supplied by American Lecithin (Oxford, CT, USA). Distearoylphosphatidylethanolamine-polyethylene glycol (DSPE-PEG) with an average molecular weight of 5,000 was provided by Nippon Oil (Tokyo, Japan). Soyaethyl morpholinium ethosulfate (SME, Forestall®) was from Croda (East Yorkshire, UK). Carboxylic acid-conjugated QDs (Qdot® 800 ITK) with emission maxima at 800 nm were provided by Invitrogen (Carlsbad, CA, USA). 4′,6-Diamidine-2-phenylindole (DAPI) was purchased from Kirkegaard and Perry Lab (Gaithersburg, MD, USA).

Preparation of Quantiosomes

Quantiosomes were prepared by a thin-film hydration technique. Span 60 (0.34%), cholesterol (0.3%), QDs (0.2%), and carboplatin (0.1%) were dissolved in a chloroform: ethanol (1:1) solvent. SPC, DSPE-PEG, or SME (0.1%) was added in the mixture if necessary. The organic solvent was evaporated by a rotary evaporator at 60°C. Solvent trace was expelled under vacuum for 4 h. The film was hydrated by pure water (8.96 ml) and then heated in water bath at 85°C for 15 min. The mixture was homogenized by high-shear homogenizer (Pro250, Pro Scientific, Monroe, CT, USA) for 10 min. Finally, a probe sonicator (VCX600, Sonics and Materials, Newtown, CT, USA) was used to further homogenate the mixture for 10 min. The total volume of the final quantiosome dispersion was 10 ml.

Vesicle Size and Zeta Potential

The mean diameter and zeta potential of quantiosomes were assessed by a laser scattering method (Nano ZS90, Malvern, Worcestershire, UK). The nanocarriers were diluted 100-fold with water before detection. The measurement was repeated three times each sample for three batches.

Carboplatin Encapsulation Percentage

Carboplatin entrapment in quantiosomes was examined by ultracentrifugation technique (Optima MAX, Beckman Coulter, Fullerton, CA, USA). The nanosystems were centrifuged at 48,000 × *g* and 4°C for 30 min for dividing the loaded drug from free form. The supernatant and precipitate were withdrawn and analyzed by atomic absorption spectrophotometer (Z5000, Hitachi, Tokyo, Japan).

Transmission Electron Microscopy (TEM)

The morphology of quantiosomes was observed by TEM (H7500, Hitachi). One drop of the nanosystems was positioned on a carbon-film-coated copper grid to form a thin-film specimen, which was then stained with phosphotungstic acid (1%). The prepared samples were examined and photographed under microscopy.

Molecular Environment

The molecular environment (polarity) of quantiosomes with different components were examined by fluorescence spectrophotometer (F2500, Hitachi) according to solvatochromism of Nile red. Quantiosomes were loaded with Nile red (1 ppm). The emission spectra of Nile red in nanocarriers were scanned from 550 to 700 nm with slit widths set to 10 nm. The excitation wavelength was set to 546 nm.

Carboplatin Release from Quantiosomes

The release of carboplatin was detected using Franz cells. A cellulose membrane (Cellu-Sep® T1, with a molecular weight cutoff of 3,500) was mounted between donor and receptor compartments. There was a 0.5-ml carboplatin (0.1%)-containing vehicle in the donor. The receptor medium consisted of 5.5 ml of pH 7.4 citrate-phosphate buffer. The available release area was 0.785 cm^2. The stirring rate and temperature were respectively set to 600 rpm and 37°C. A 300-μl aliquot was sampled from receptor at appropriate intervals and then replaced with an equal volume of medium. The drug amount in receptor was analyzed by atomic absorption spectrophotometer.

Cell Lines

Both mouse melanoma B16F0 cell line and ovarian cancer ES-2 cell line were supplied by American Type Culture Collection (Rockville, MD, USA).

Cellular Uptake

The procedures for cell culture were carried out based on previous studies (15,16). The cells were plated at 2×10^5 cells/well for 8 h incubation. Quantiosomes were added to the wells and incubated for 4 h at 37°C. Cells were washed three times with phosphate-buffered saline (PBS). DAPI (100 ng/ml) was pipetted into cell medium for staining nuclei. The cellular uptake of nanocarriers was observed by an inverted fluorescence microscope (IX81, Olympus, Tokyo, Japan). The wavelengths of excitation and emission were 405 and 800 nm, respectively.

Cytotoxicity Assay

Quantiosomes with carboplatin at a final concentration of 100 μM were added to confluent cells grown in plates after DMEM dilution. The plate was incubated at 37°C for 24 h. After saline wash, the cells were incubated with 3-(4,5-dimethylthiazol-2-yl)-2,5-diphenyl tetrazolium bromide (MTT, 5 mg/ml) in RPMI-1640 for 2 h. Formazan crystals resulting from MTT reduction were dissolved by adding DMSO with agitation for 30 min. The UV absorbance of supernatant was determined at 550 nm. Cell viability was calculated as a percentage of a non-treatment control.

Cell Migration

Cell mobility of melanoma cells was evaluated by cell migration and movement. Cells were seeded at 2×10^5 cells/well in plates. After formation of a monolayer, a wound was created by scratching a line with a micropipette tip. Cell debris was washed away with PBS. Melanoma cells were exposed to quantiosomes at a 1:100 dilution. Wound closure was imaged 48 h after incubation.

Animals

Female nude mice (ICR-Foxn1nu) aged 8 weeks old were purchased from National Laboratory Animal Center (Taipei, Taiwan). The animal experimental protocol was reviewed and approved by Institutional Animal Care and Use Committee of Chang Gung University. A 300-μl medium (10% fetal bovine serum, 89% DMEM, and 1% penicillin-streptomycin) with melanoma cells (10^6 cells) was subcutaneously administered into both sites of dorsal area. When the tumor had grown to ~250 mm^3, the mouse was employed for *in-vivo* experiments. The total animals used in this study were 48.

Intratumoral Drug Concentration

The mouse was anesthetized with isoflurane. The solution of quantiosomes (50 μl) with carboplatin (50 μg) was directly injected into the solid tumors. Saline was injected to tumors

on the other side of the dorsal area for comparison. After a 24-h administration, the animal was sacrificed and the tumors were excised and weighed. The tumors were added in test tubes and homogenized with methanol (1 ml) at 700 rpm for 5 min. The resulting mixture was centrifuged at 3,000×*g* for 10 min. The carboplatin amount in supernatant was detected by atomic absorption spectrophotometer.

In-Vivo Real-Time Bioimaging

In-vivo fluorescence imaging of melanomas and ovary tumors was visualized by a Pearl® Impulse System (Li-Cor, Lincoln, NE, USA). After intratumoral injection of free QDs or quantiosomes (50 μl with 0.1% carboplatin) into tumors, the animals were fixed in a light-tight chamber. A gray-scale reference image was obtained under a low-level signal. The optical emission was set to 800 nm. Images were photographed before administration, and 0, 1, 2, 4, 6, 12, 24 h after injection. The tumors were removed and washed with saline. The fluorescence imaging of excised tumors was photographed in the imaging system.

Statistical Analysis

Statistical analysis of the differences between different treatments was carried out using unpaired *t*-test with Dunn's post-test. A 0.05 level of probability ($p<0.05$) was taken as the level of significance. Data entry and calculation was completed by using Winks version 6 (Texasoft, Duncanville, TX, USA).

RESULTS

Physicochemical Characterization of Quantiosomes

We had prepared four formulations of quantiosomes, including plain, SPC-loaded, PEGylated, and positively charged systems. In all cases, 156 μmol Span 60/cholesterol (1:1) was mixed with 10 mg carboplatin to form a final product of 10 ml. Table I summarizes the physicochemical properties of these four nanosystems. A hydrodynamic diameter of 177 nm was determined for plain quantiosomes. A slight but significant decrease ($p<0.05$) in the mean diameter was observed after loading other additives. The results showed that the average size of quantiosomes with SPC, PEG, and SME was 167, 173, and 151 nm, respectively. The polydispersity index (PDI) was low for all systems (≤ 0.25), revealing a narrow size distribution. The vesicle size of quantiosomes was also examined in the absence of QDs as listed in Table II. The carboxyl QDs utilized in this work exhibited a size of 18 nm according to the manufacturer's profile. Interestingly, the exclusion of QDs resulted in some increase ($p<0.05$) of the vesicle diameter for plain, PEGylated, and positively charged formulations. The conjugation of QDs did not alter the size of SPC-loaded nanocarriers ($p>0.05$).

Table I The Characterization of the Quantiosomes by Particle Diameter, Polydispersity Index (PDI), Zeta Potential, and Carboplatin Encapsulation Percentage

Formulation	Size (nm)	PDI[a]	Zeta potential (mV)	Encapsulation (%)
Plain	176.9 ± 1.1	0.18 ± 0.01	−51.1 ± 1.8	43.2 ± 2.2
SPC	167.0 ± 1.2	0.25 ± 0.08	−24.6 ± 1.6	50.6 ± 3.0
PEGylation	172.9 ± 0.9	0.22 ± 0.11	−31.6 ± 1.1	46.9 ± 2.0
Positive charge	151.0 ± 1.0	0.21 ± 0.07	12.5 ± 1.0	58.2 ± 2.1

[a] *PDI* polydispersity index

Each value represents the mean ± SD ($n=3$ for size, PDI and zeta potential, $n=4$ for drug encapsulation)

The surface of the plain quantiosomes was negatively charged (−51 mV) as shown in Table I. The negative zeta potential of quantiosomes by incorporating with SPC was reduced to −25 mV ($p<0.05$). A similar result was observed for PEGylated quantiosomes (−32 mV). SME-coated vesicles had a zeta potential of +13 mV. Quantiosomes with various modifications allowed the encapsulation of carboplatin. Different formulations showed a carboplatin-loading capacity of >45%. As reported in Table I, encapsulation percentages were found to be 43%, 51%, 47%, and 58% for plain, SPC, PEG, and SME, respectively. It was obvious that formulations with modification could achieve greater entrapment than plain vesicles, with positively charged dispersions showing the highest value ($p<0.05$). We had previously evaluated the storage stability of quantiosomes in the environment of 40°C and 75% relative humidity based on the guidelines of International Conference on Harmonization (ICH). The results showed that the size and zeta potential of quantiosomes was not changed during a 1-month period (data not shown).

Figure 1 depicts TEM images of quantiosomes formulated using various additives. The upper panel of Fig. 1a to d represents plain, SPC, PEGylated, and cationic quantiosomes without QDs. The lower panel of this figure demonstrates images of quantiosomes containing QDs. The presence of multiple bilayers is observed from TEM images (arrows) of a single vesicle, especially for plain and SPC quantiosomes (Fig. 1a and b). The prepared niosomes appeared as spherical vesicles. It can be

Table II Particle Size of Quantiosomes Without Quantum Dots in the Nanosystems

Formulation	Size (nm)
Plain	206.6 ± 2.4
SPC	165.4 ± 1.3
PEGylation	178.9 ± 0.3
Positive charge	202.1 ± 1.1

Each value represents the mean ± SD (n = 3)

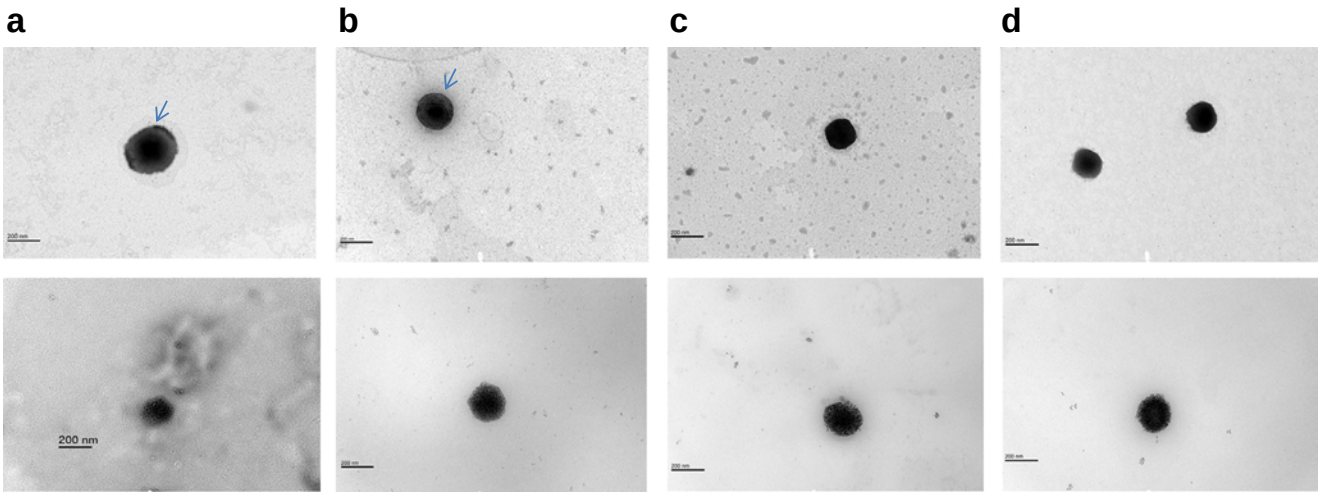

Figure 1 Transmission electron microscopic (TEM) photographs of (**a**) plain quantiosomes, (**b**) SPC-loaded quantiosomes, (**c**) PEGylated quantiosomes, and (**d**) cationic quantiosomes. The upper panel is the image of quantiosomes without quantum dots (QDs). The lower panel is the image of quantiosomes containing QDs. The scale bar is 200 nm.

clearly observed that QDs were distributed throughout the bilayers of the quantiosomes with a high density. Vesicles maintained a spherical shape after QD insertion. The observed size for individual vesicles was approximated to that determined by laser scattering. The molecular environment (polarity) of different formulations was examined by detecting Nile red emission as shown in Fig. 2. Nile red is very soluble in a lipophilic environment and reveals strong fluorescence intensity. On the other hand, the increase in environmental polarity (hydrophilicity) would produce the aggregation of Nile red, resulting in the quenching of fluorescence. Plain quantiosomes showed the highest intensity near 580 nm, followed by PEG, SPC, and cationic formulations. This suggests that the greatest lipophilicity of the nanosystems occurs in plain vesicles. On the other hand, quantiosomes containing SME exhibited the lowest lipophilicity of the nanodispersions.

Carboplatin Release from Quantiosomes

The release amount-time curves of carboplatin from quantiosomes are depicted in Fig. 3. The discrepancy of release rate between different formulations was not large. SPC-containing quantiosomes showed the highest carboplatin release compared to other nanocarriers ($p<0.05$). There was no significant difference ($p>0.05$) among the release of plain, PEGylated, and cationic systems. Carboplatin release revealed an initial burst, followed by a gradual leveling off after 10 h. The burst effect could be due to the non-encapsulated carboplatin (about 50% of the total drug added) outside niosomal vesicles. These drug molecules quickly and freely diffused from donor to receptor compartment.

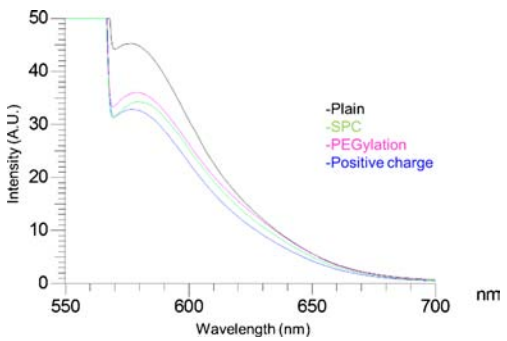

Figure 2 Fluorescence emission profiles of Nile red in quantiosomes. The emission fluorescence spectra of Nile red were scanned from 550 to 700 nm with both slit widths set to 10 nm.

In-Vitro Cellular Uptake, Cytotoxicity, and Migration

In-vitro cellular uptake of quantiosomes was monitored in melanoma cells as shown in Fig. 4. Carboplatin was not added in nanodispersions in this experiment. Cell nuclei were stained blue by DAPI. Figure 4a shows melanoma cells incubated with only

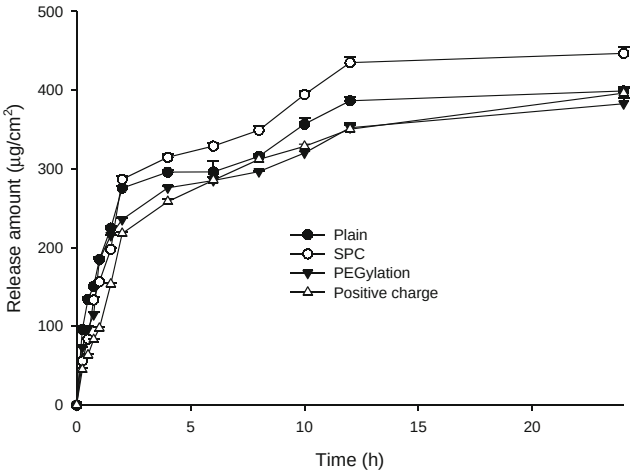

Figure 3 Carboplatin release ($\mu g/cm^2$) across a cellulose membrane from quantiosomes. $n=4 \pm$ SD.

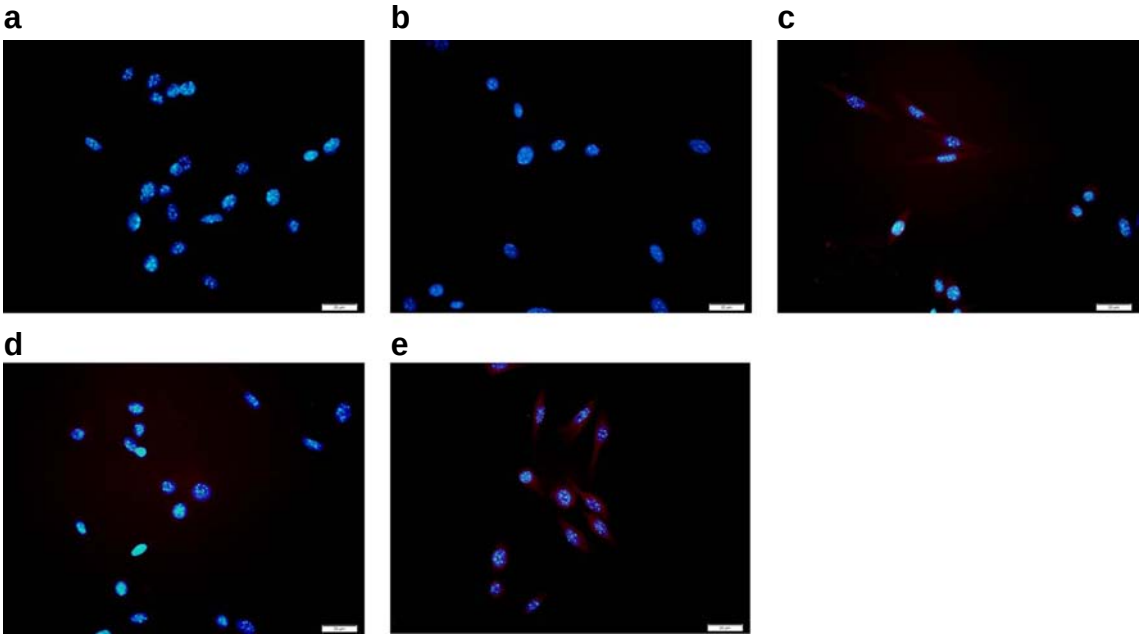

Figure 4 Fluorescence microscopic images of melanoma cell (B16-F0) internalization by (**a**) saline, (**b**) plain quantiosomes, (**c**) SPC-loaded quantiosomes, (**d**) PEGylated quantiosomes, and (**e**) cationic quantiosomes.

PBS. Intrinsic red fluorescence of the cells at the near-infrared wavelength was low, indicating the absence of interference from native cell fluorescence. The cellular uptake was a function of the surface structure of the quantiosomes. A negligible internalization of melanoma cells by treatment with plain quantiosomes was observed (Fig. 4b). Red fluorescence was visible in the cytoplasm after treatment with SPC-loaded quantiosomes (Fig. 4c), suggesting the delivery of QDs into the cells. The red signal in the cytoplasm was also observed for the PEGylated systems (Fig. 4d), although the fluorescence intensity was fainter than that of the SPC systems. A remarkable internalization was shown for cationic quantiosomes (Fig. 4e). The signal could be imaged throughout the cytoplasm and the perinuclear regions. The results of cellular uptake provided evidences that quantiosomes could target melanoma cells. In the absence of carboplatin, no signs of morphological alteration to the cells were demonstrated upon treatment of these nanosystems. This implies a low cytotoxicity of the vesicles themselves.

Cytotoxic activity against melanoma was evaluated as shown in Fig. 5. No cytotoxicity was revealed for drug-free nanosystems (data not shown), suggesting the nanocomposites did not influence carboplatin action. Melanoma cell viability displayed a level of 52% by treatment with carboplatin in aqueous solution, which was near the value of IC_{50}. The improvement of carboplatin cytotoxicity was preferred by loading with quantiosomes. The growth-inhibitory activity of niosomal carboplatin was 3 to 4 times stronger than that of free carboplatin. All quantiosomes showed a comparable viability ($p > 0.05$).

The migration characteristic of melanoma was investigated by treating quantiosomes with carboplatin as shown in Fig. 6. The cells that underwent no treatment would migrate to close the cell-free zone after a 48-h incubation (Fig. 6a). Migratory cells were completely inhibited by free carboplatin in aqueous control (Fig. 6b). The same result was recognized for plain, SPC, and PEG quantiosomes (Fig. 6c to e). There were some migrated cells in the group of cationic quantiosomes after 48 h of treatment (Fig. 6f), indicating a less-inhibitory effect on cell motility compared to other quantiosomes.

In-Vivo Intratumoral Drug Concentration and Bioimaging

A more complicated *in-vivo* tumor model was created for examining the therapeutic efficiency of drug-loaded

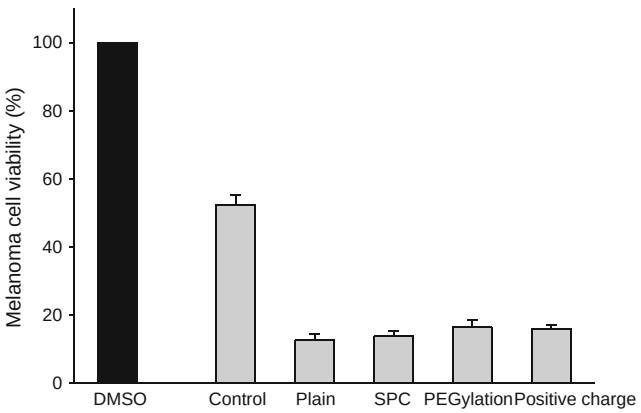

Figure 5 Viability of melanoma cells (B16-F0) after treatment with carboplatin-loaded quantiosomes at 100 μM. $n = 3 \pm$ SD.

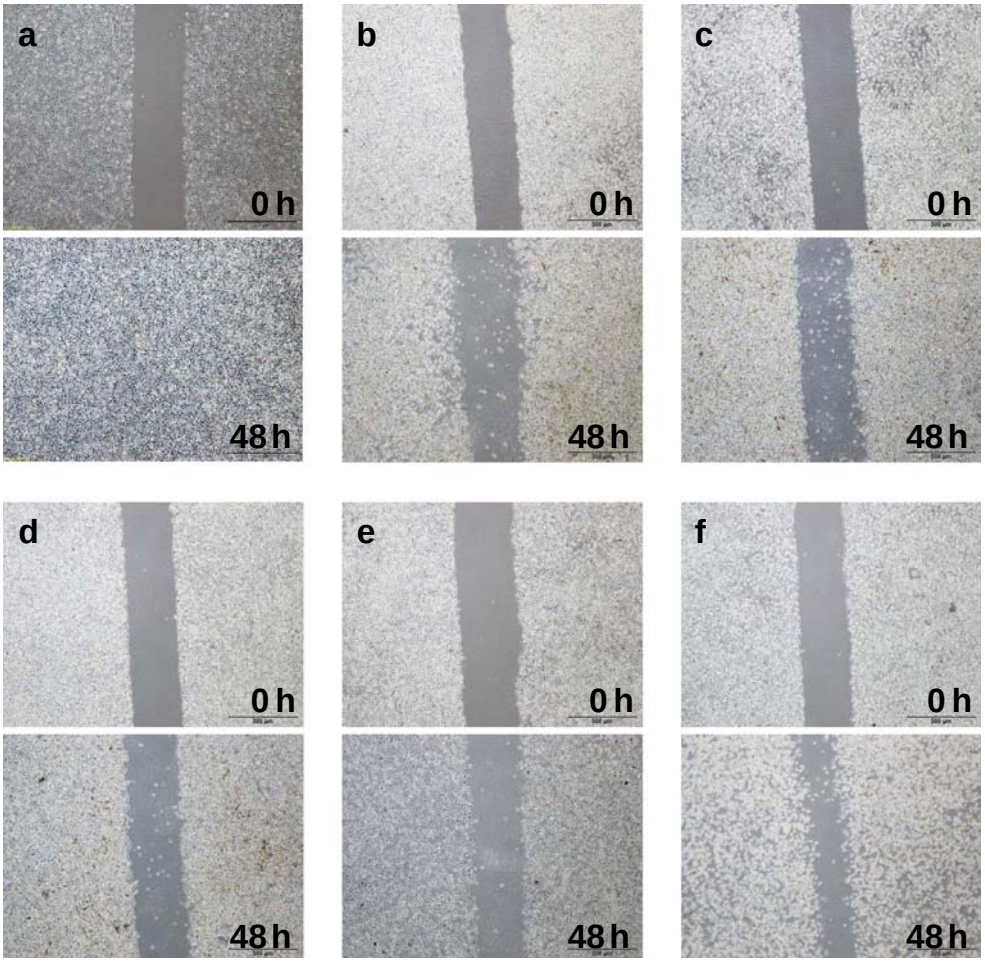

Figure 6 Migration of melanoma cells (B16-F0) before and after incubation with (**a**) saline, (**b**) carboplatin in aqueous solution, (**c**) plain quantiosomes, (**d**) SPC-loaded quantiosomes, (**e**) PEGylated quantiosomes, and (**f**) cationic quantiosomes.

quantiosomes. Carboplatin in aqueous dispersion or quantiosomes was intratumorally injected into melanoma. The tumors were excised at 24 h after injection for measuring the drug content. As compared to the aqueous control, plain and positively charged vesicles did not increase the carboplatin concentration in tumors (Fig. 7). The accumulation of the drug in melanoma had been enhanced by the preparations with SPC and PEG. The carboplatin concentration was increased from 6.29 to 9.43 and 9.99 ng/mg by loading into the SPC- and PEG-containing formulations, respectively.

Quantiosomes containing SPC and PEG were selected for *in-vivo* real-time imaging because of their ability to enhance carboplatin tumor delivery. As illustrated in Fig. 8, fluorescence images of nude mice were obtained at different time points after intratumoral injection of free QDs and quantiosomes. Nanosystems and saline were respectively applied in the left- and right-side melanomas. As shown in Fig. 8a, a localization of free QDs was confirmed by a bright field in the left-sided tumor. The fluorescence intensity gradually decreased following the increase of time. A weak signal was still seen at 24 h post injection. However, the fluorescence was mainly located in the peri-tumor regions but not within the tumors. The right panel of Fig. 8 demonstrates imaging of the excised tumors and the mouse body 24-h post injection. No fluorescence in the tumor was observed for the free control. There were some green signals in the normal tissues after

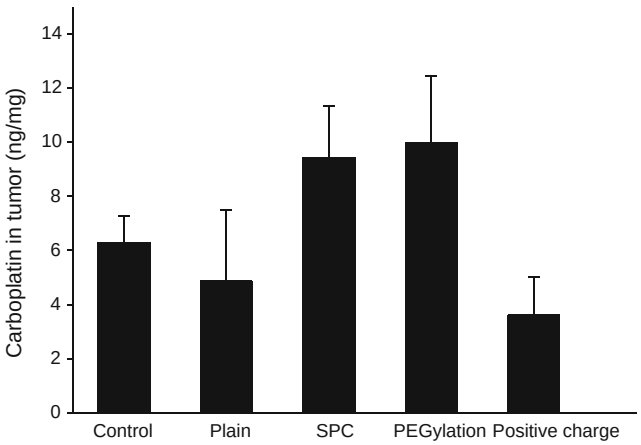

Figure 7 Carboplatin amount (ng/mg) in melanoma tumor after intratumor injection of aqueous solution and quantiosomes containing carboplatin. $n = 6 \pm$ SD.

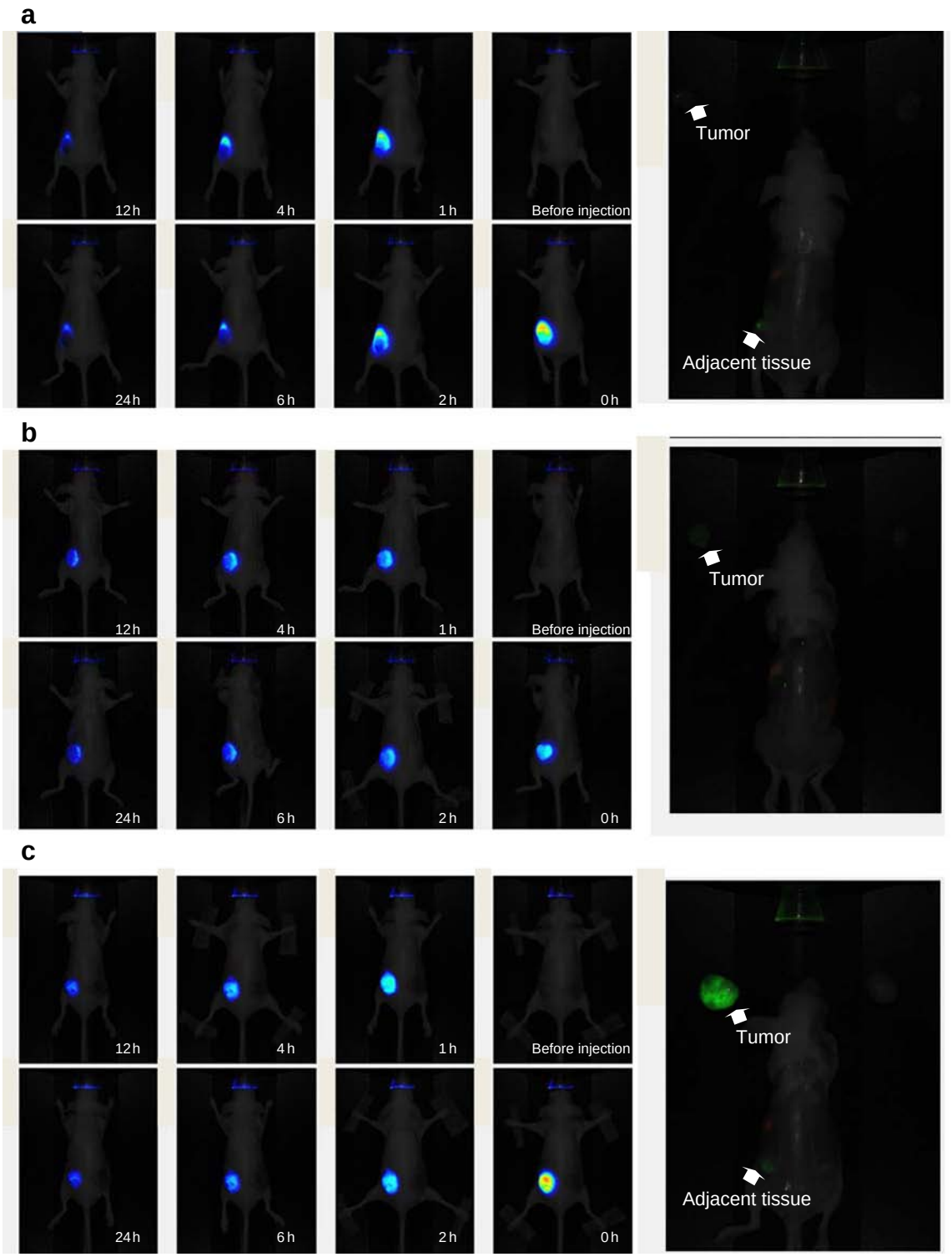

Figure 8 Fluorescence imaging of melanoma-bearing nude mice detected with the *in-vivo* imaging system following an intratumor injection of (**a**) free QDs, (**b**) SPC quantiosomes, and (**c**) PEGylated quantiosomes. Tumor on the left side was injected with nanosystems. Tumor on the right side was injected with saline as a control. The right panel of each figure is the fluorescence imaging of excised tumors and the adjacent area after a 24-h administration.

removing the tumor. This indicated a quick diffusion of carboxyl QDs from the tumor site to the surrounding area. With respect to two quantiosomes tested (Fig. 8b and c), a stronger fluorescence persisted to 24 h as compared to free QDs. A weak fluorescence signal was visualized at the tumor site after excision of the tumor treated with SPC formulations, indicating that this nanocarrier was selectively maintained in the tumor tissue. No signal was found in normal tissue around

the tumor area. A brighter signal was observable by the resected tumor treated with PEGylated formulations, although the adjacent tissue also displayed a weak mark.

Cytotoxicity and *in-Vivo* Bioimaging of Ovarian Cancer

In order to expand the usefulness of quantiosomes, ovarian cancer cells were utilized as another cancer model for examining cytotoxicity and *in-vivo* bioimaging. Carboplatin-containing quantiosomes at a concentration of 100 μM reduced ovarian cancer cell viability to ~35%, which was 2-fold lower with respect to the data of the aqueous control as shown in Fig. 9. As with melanoma cells, there was no significant difference ($p > 0.05$) among cytotoxicity of different nanodispersions. Although intratumoral administration is inapplicable to ovarian cancer therapy and imaging in real clinical situations, we still used this model to test the retention ability of quantiosomes in tumor sites. As shown in Fig. 10, the left- and right-side ovarian tumors were respectively injected with saline and nanocomposites. Though a momentous fluorescence was detected immediately after injecting free QDs into the tumors, the signal was quickly diminished as soon as the 2 h post-injection point was reached (Fig. 10a). Decoration of quantiosomes with SPC and PEG improved QD retention in tumors (Fig. 10b and c). The decay of fluorescence was not significant during the 24 h period. The excised tumor treated by free QDs showed no fluorescence signal. On the other hand, an appreciable signal was revealed for the groups of quantiosomes. A faint but observable fluorescence was also detected in normal tissues near the tumors.

DISCUSSION

Cutaneous melanoma is a complex tumor with a heterogeneous aetiology of which the incidence continues to increase. A nanomedical approach may potentially enhance early diagnosis, therapy, and prognosis of melanoma. In this study, we developed novel multifunctional nanocarriers to identify melanoma, and we explored the therapeutic efficacy of the nanosystems *in-vitro* and *in-vivo*. Quantiosomes with various modifications exhibited much improved cytotoxic activity against melanoma. These vesicles could efficiently deliver QDs into the cytoplasm for a sensitive labeling of the cells. An enhanced delivery was also detected in the *in-vivo* intratumoral carboplatin concentration by quantiosomes. This nanocarrier could accumulate QDs in the tumors for a prolonged duration (24 h). The successful performance of quantiosomes was also achieved for ovarian cancers, indicating the extensive applicability of the nanosystems.

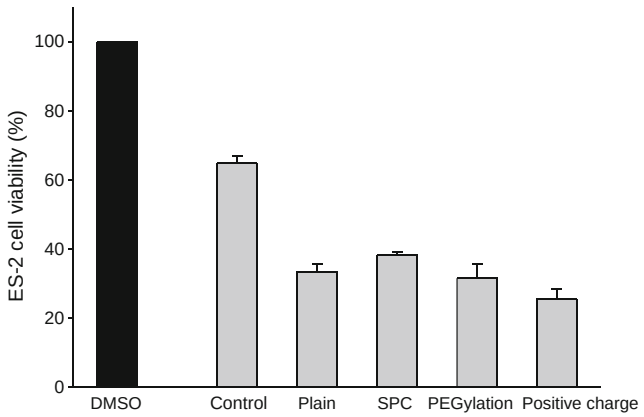

Figure 9 Viability of ovarian cancer cells (ES-2) after treatment with carboplatin-loaded quantiosomes at 100 μM. $n = 3 \pm$ SD.

Quantiosomes were mainly derived from niosomes, which showed a structure of a closed bilayer vesicle with an aqueous core. Span 60 and cholesterol were the fundamental materials of quantiosomes. Span 60, a sorbitan ester, was selected because of its ideal entrapment efficiency and sustained release for the encapsulated drugs proven previously (17,18). It is widely used as surfactants in pharmaceutics and foods. Cholesterol is able to prevent drug leakage from niosomes. Span 60 and cholesterol form niosomal bilayers by hydrogen binding (19). To render the QDs soluble in aqueous dispersion, carboxyl-functionalized QDs were employed for noisome loading for forming quantiosomes. SPC, PEG, or SME was added to quantiosomes for further formulation design. SPC loading in vesicles may simulate the structure and property of liposomes. PEGylation could avoid elimination by the immune system and prolong its half-life in the body (20). PEG also showed biocompatibility to minimize the toxicity of QDs (21). SME provided a positive charge for quantiosomes to enhance the interaction and fusion between vesicles and cell membranes.

All modifications to plain quantiosomes led to the reduction of vesicle size. This could be due to SPC, DSPE-PEG, and SME possessing an amphiphilic property as emulsifiers for further stabilizing vesicles. The long PEG chains on the vesicular surface may result in enlargement of the liposomal dimension (22). This is not the case in the present study. DSPE-PEG, composed of lipophilic phospholipid and hydrophilic PEG moiety, offered an amphiphilic character to decrease vesicle size. Another observation was that the conjugation of QDs in niosomes elicited a size reduction. This demonstrated that carboxyl QDs might possess an emulsifier competence on the bilayers. According to TEM images, QDs were located in the bilayer membrane of the quantiosomes. The interaction between QDs and the bilayers resulted in the decreased size. This incorporation generally did not disrupt the structure of the quantiosomes. Some ionization occurred for QDs with the carboxyl group in aqueous dispersion (23). This contributed to a negative surface charge of plain quantiosomes. SPC and PEG could shield some negative charge in the quantiosomes, which was due to the dilution of

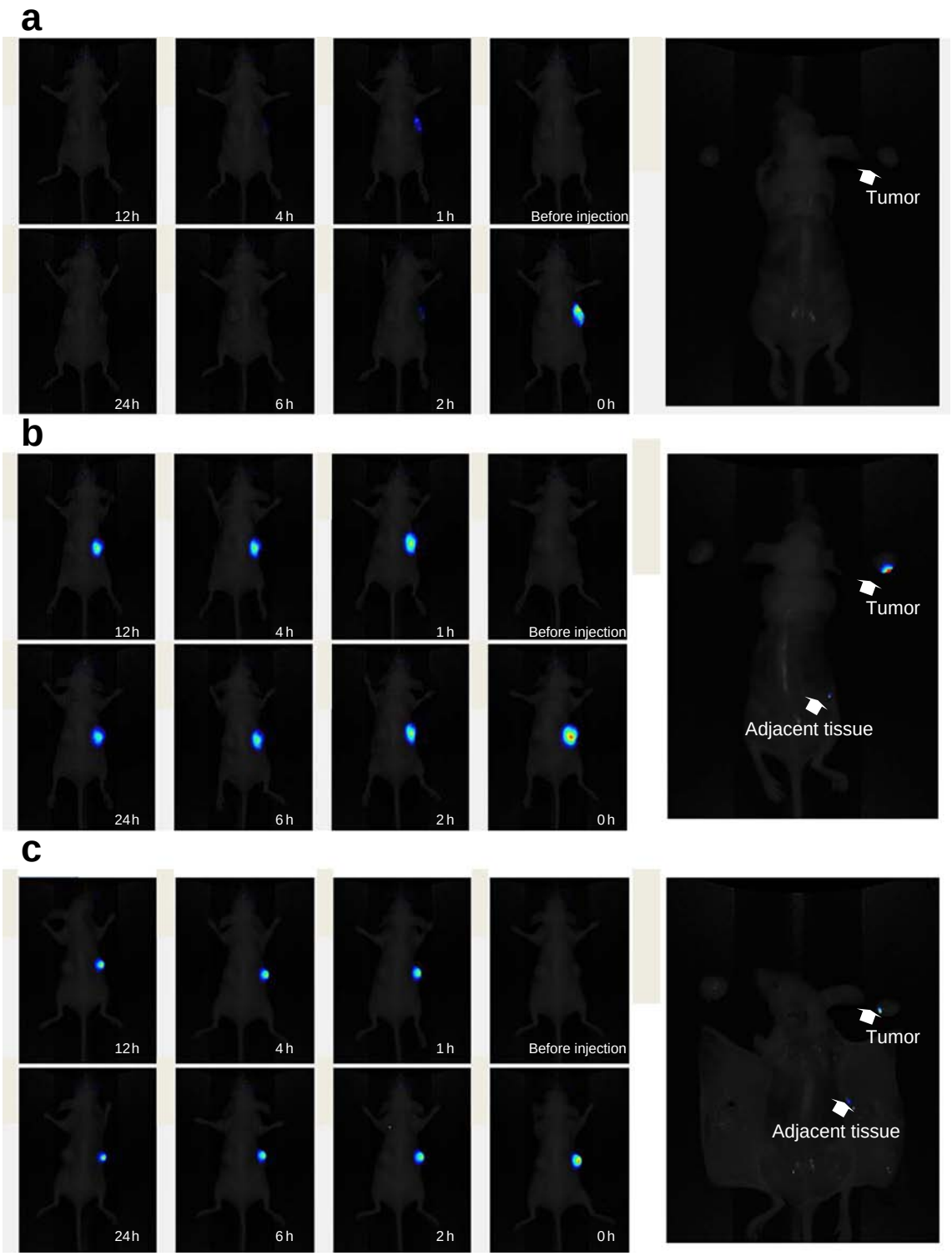

Figure 10 Fluorescence imaging of ovarian tumor-bearing nude mice detected with the *in-vivo* imaging system following an intratumor injection of (**a**) free QDs, (**b**) SPC quantiosomes, and (**c**) PEGylated quantiosomes. Tumor on the left side was injected with nanosystems. Tumor on the right side was injected with saline as a control. The right panel of each figure is the fluorescence imaging of excised tumors and the adjacent area after a 24-h administration.

QD concentration in the bilayers after adding SPC and PEG. It confirmed the presence of SPC or DSPE-PEG on the niosomal surface. SME gave a positive charge of quantiosomes as expected. Nile red fluorescence would be quenched in a hydrophilic environment. It was found that the incorporation of SPC, DSPE-PEG, and SME had increased the hydrophilicity of the quantiosomes. All of these additives hold hydrophilic moieties such as ester groups,

hydroxyl groups, or morpholin. This could lead to an increased hydrophilicity.

Carboplatin showed an octanol/water partition coefficient (log *P*) of −0.46 (24), which could be categorized as a hydrophilic drug. About 50% of the carboplatin molecules in nanosystems could be entrapped into vesicles. Both Span 60 and cholesterol have hydroxyl moieties. There are two amines in the carboplatin structure. The hydrogen bonds formed in bilayers to interact with the amphiphile head groups of Span 60/cholesterol and the drug. The possible interaction between carboplatin and hydrophilic moiety of SPC, DSPE-PEG, and SME had further promoted drug encapsulation. The aqueous core could be another compartment for carboplatin residence in addition to the niosomal membrane. Our results suggested that quantiosomes provide a feasible way to load both QDs and the drug.

A greater uptake of nanoparticles by tumor cells contributes to better efficiency of molecular imaging. Our previous study had demonstrated a difficulty of melanoma cell uptake by carboxyl QDs (15). It is plausible since the fluorescence of QDs was quenched as endosomes and lysosomes entrapped QDs (25). Carboxyl QDs always aggregate in cytosol due to poor stability in an acidic environment (26). A failure of QDs uptake by melanoma cells was also demonstrated in a previous study (27). Quantiosomes after modification could improve cellular uptake of QDs. Niosomes can interact with cells and fuse with the cell membrane because of the fluidity of the bilayers (28). As observed in TEM, one single vesicle carried numerous QDs on the surface. Quantiosomes would offer a high QD-concentration gradient toward the cells. Subsequently, niosomes may release QDs directly into the cytoplasm. This improvement was not recognized for plain systems. The lipophilic nature of quantiosomes could impact cell fusion. Since plain formulations showed the least lipophilicity based on Nile red emission profiles, the fusion to lipophilic plasma membrane would be retarded. Another possibility was the highest negative charge of plain systems. Since the cell membrane carried a negative charge, repulsion between plain quantiosomes and cells occurred. Zeta potential also suggested an excellent internalizing ability of positively charged vesicles due to electrostatic interaction with the cell membrane. Although SPC and PEG quantiosomes possessed a negative charge, they delivered QDs to cells to a certain level. Furthermore, the steric hindrance of PEG on a nanoparticulate surface often minimizes membrane fusion (29). There must be other factors besides lipophilicity governing the cellular uptake of PEGylated niosomes. Dioleoyl phosphatidylethanolamine (DOPE) is well-known as a fusogenic lipid for promoting membrane fusion (23). PE moiety in DSPE-PEG might have the same benefit. PEG accelerates cellular endocytosis via a low-density lipoprotein receptor (30). Cosco et al. (31) also demonstrated that PEG-coated niosomes interact with the membrane of MCF-7 breast cancer cells.

A cytotoxicity test of melanoma showed that quantiosomes augmented the growth-inhibitory effect of carboplatin by 3 ~ 4-fold. In the case of ovarian cancer cells, quantiosomes had a cytotoxic activity two orders of magnitude greater than the control group. This might be a result of increased uptake to cancer cells. Nevertheless, it cannot explain the comparable cytotoxicity of plain nanocarriers, which showed a negligible uptake, to other formulations. Half of the carboplatin molecules in nanodispersions were not entrapped by vesicles. The free drug might directly interact with cells to induce apoptosis. The main reason for the enhanced cytotoxicity could be that carboplatin was slowly released from the vesicles for prolonged delivery. As shown in the drug release profiles, the initial burst of carboplatin provided a high dose to treat cancer cells in the beginning. The subsequent release in a sustained manner could maintain the cytotoxic effect. Quantiosomes may offer an advantage of achieving the same cytotoxicity against cancer cells with a lower carboplatin dose compared to the free control. The multifunctional quantiosomes delivered both the imaging agent and the drug at a high concentration to cells according to experiments involving cell uptake and cytotoxicity. Metastatic melanoma is a serious concern nowadays due to the failure of the numerous regimens (32). A predominant characteristic of metastasis is cancer cell migration. Our results showed that free carboplatin totally inhibited melanoma migration during a 48 h period. Carboplatin incorporation in quantiosomes maintained the restrained migration activity.

For effective chemotherapy and monitoring, a high concentration of anticancer drugs and imaging agents is required at the tumor site. This approach reduces drug concentration in other tissues, thus minimizing adverse reaction. Intratumoral injection, which provides this advantage, is suitable for superficial and well-localized tumors, such as melanoma (33,34). SPC and PEGylated quantiosomes provided a higher carboplatin accumulation in melanoma compared to the free control after intratumor administration. This could be a consequence of favored maintenance of quantiosomes inside the tumors. This result was not compatible to cellular uptake experiment, which demonstrated significant internalization by SPC and cationic systems. PEGylated vesicles might accumulate in extracellular matrix of tumor site. The depot of the niosomal drug within the tumors resulted in a prolonged and sustained delivery of carboplatin. This phenomenon was not detected by plain and cationic preparations. Cationic nanoparticles show fast clearance in the complicated body fluid environment (34). A previous study (35) also suggests a drastic increase in clearance for cationic niosomes in body fluid. Although cationic nanosystems were easily internalized into cytoplasm of melanoma cells, they are of no use unless the vesicles could largely retain in tumor site and then penetrate into cells.

One of the advantages of QDs for imaging *in-vivo* is the deeper penetration of the signal and higher photostability compared to organic dyes (1). However, QDs usually show restrained retention in tumor cells even after intratumor injection (23,36). This low accumulation of fluorescence derived from free QDs was confirmed in this study. Tumor-associated vasculatures are highly permeable, showing enhanced permeability and retention (EPR) (37). The small nanoparticles of <100 nm can freely transport through the blood vessels in tumors. The real-time imaging and excised tumors reveal a leakage of QDs from the tumor site to surrounding tissues, possibly leading to adverse reaction and systemic toxicity. Carboxyl QDs easily drain toward the lymph node in the tumor-bearing area (38), resulting in the loss of QDs from the tumor. Protein adsorption also quenches the fluorescence of QDs (25). The profiles of *in-vivo* bioimaging showed that SPC and PEG quantiosomes were stable under physiological conditions. Quantiosomes were principally confined to tumors in a prolonged manner for at least 24 h after intratumor injection. PEGylated quantiosomes represented the highest retention in tumors. The steric structure of PEG significantly reduces protein bonding and inhibits vesicle aggregation in serum or tissue fluid (35,39). Thus, the half-life and constancy in the *in-vivo* harsh environment were ameliorated.

Coexistence of QDs and carboplatin in niosomes was favorable for labeling and therapy of melanoma and ovarian cancer based on the experimental data in this work. Quantiosomes were well distributed in tumors and demonstrated a longer retention time for tracking tumors. Poor biocompatibility and potential toxicity of QDs lead to the limited application for *in-vitro* and clinical studies. The toxicity greatly depends on doses (26). The possibility of reducing the QD amount by application of quantiosomes for efficient bioimaging can be anticipated, thus alleviating the toxicity. Decreasing the QDs used also reduces the cost. Moreover, the cost of fluorescence imaging is generally lower than that of positron emission tomography (PET) and single-photon emission computed tomography (40). Currently, several commercial liposomes are available for cancer diagnosis and therapy. The cost of these nanomedicines is very high due to the cost of materials for preparing liposomes. The price of phosphatidylcholine (purity >99%) supplied by Sigma-Aldrich (August 2013) was $589 in United States dollars (USD) per 1 g. A package of 250 g Span 60 cost only US$41.3. Quantiosomes developed in this report may imply a high capability/price (C/P) for efficient use as a multifunctional nanocarrier. We had previously employed QDs for inclusion into liposomes and nanostructured lipid carriers (NLCs) to observe and treat tumors (15,41). All of these nanosystems could prolong the fluorescence in tumors for at least 24 h. As described above, niosomes containing QDs as a multifunctional nanocarrier are potential for application due to the lower cost and easier preparation compared to other nanosystems. According to the data in the present work, we demonstrated the physicochemical stability, reproducibility of drug release, and the influence of formulations of quantiosomes as critical issues of evaluating the industrial and clinical applicability. The present report encourages further development of quantiosomes for scale-up in industries.

CONCLUSIONS

In this study we have developed novel multimodal nanocomposites based on niosomal systems for bioimaging and drug delivery. Clearly, quantiosomes exhibited different *in-vitro* and *in-vivo* profiles compared to free QDs and carboplatin. Quantiosomes could efficiently facilitate cellular uptake of QDs for biolabeling. The cytotoxicity against melanoma and ovarian cancer cells was increased by incorporating carboplatin into the vesicles. The experimental results showed that quantiosomes increased intratumoral carboplatin concentration in tumors. The sensitive and sustained fluorescence imaging using quantiosomes as probes could dramatically monitor the tumors at the living-mouse level. The carrier composition, vesicle size, surface charge, and polarity played roles in bioimaging and in the drug delivery of quantiosomes. The nanosystems demonstrated herein permit further development of cancer-management strategy for early diagnosis and therapeutics. Future work is needed to design quantiosomes with targeted ability to cancers, such as conjugation of antibodies or peptides, so that the quantiosomes can be administered intravenously for extensive application.

ACKNOWLEDGMENTS AND DISCLOSURES

The authors are grateful for the financial support from Chang Gung University of Science and Technology (EZRPF3C0221).

REFERENCES

1. Wang C, Cao X, Su X. In vitro and in vivo imaging with quantum dots. Anal Bioanal Chem. 2010;397:1397–415.
2. Ghaderi S, Ramesh B, Seifalian AM. Fluorescence nanoparticles "quantum dots" as drug delivery system and their toxicity: a review. J Drug Target. 2011;19:75–486.
3. Al-Jamal WT, Kostarelos K. Liposomes: from a clinically established drug delivery system to a nanoparticle platform for theranostic nanomedicine. Acc Chem Res. 2011;44:1094–104.
4. Bothun GD, Rabideau AE, Stoner MA. Hepatoma cell uptake of cationic multifluorescent quantum dot liposomes. J Phys Chem B. 2009;113:7725–8.
5. Mukthavaram R, Wrasidlo W, Hall D, Kesari S, Makale M. Assembly and targeting of liposomal nanoparticles encapsulating quantum dots. Bioconjug Chem. 2011;22:1638–44.

6. Wen CJ, Zhang LW, Al-Suwayeh SA, Yen TC, Fang JY. Theranostic liposomes loaded with quantum dots and apomorphine for brain targeting and bioimaging. Int J Nanomedicine. 2012;7: 1599–611.
7. Joo KI, Xiao L, Liu S, Liu Y, Lee CL, Conti PS, *et al.* Crosslinked multilamellar liposomes for controlled delivery of anticancer drugs. Biomaterials. 2013;34:3098–109.
8. Kazi KM, Mandal AS, Biswas N, Guha A, Chatterjee S, Behera M, *et al.* Niosome: a future of targeted drug delivery systems. J Adv Pharm Technol Res. 2010;1:374–80.
9. Marianecci C, Rinaldi F, Mastriota M, Pieretti S, Trapasso E, Paolino D, *et al.* Anti-inflammatory activity of novel ammonium glycyrrhizinate/niosomes delivery system: human and murine models. J Control Release. 2012;164:17–25.
10. Mandel S, Banerjee C, Ghosh S, Kuchlyan J, Sarkar N. Modulation of the photophysical properties of curcumin in nonionic surfactant (Tween-20) forming micelles and niosomes: a comparative study of different microenvironments. J Phys Chem B. 2013;117:6957–68.
11. Wang Y, Chen L. Quantum dots, lighting up the research and development of nanomedicine. Nanomedicine Nanotechnol Biol Med. 2011;7:385–402.
12. Volkovova K, Bilanicova D, Bartonova A, Letašiová S, Dusinska M. Associations between environmental factors and incidence of cutaneous melanoma. Rev Environ Health. 2012;11 Suppl 1:S12.
13. Måsbäck A, Andersson G, Olsson H. Problems in assessing multiple cutaneous melanoma. A review on the accuracy of a population based cancer registry. Cancer Epidemiol. 2010;34:262–6.
14. Flaherty KT, Lee SJ, Zhao F, Schuchter LM, Flaherty L, Kefford R, *et al.* Phase III trial of carboplatin and paclitaxel with or without sorafenib in metastatic melanoma. J Clin Oncol. 2013;31:373–9.
15. Wen CJ, Sung CT, Aljuffali IA, Huang YJ, Fang JY. Nanocomposite liposomes containing quantum dots and anticancer drugs for bioimaging and therapeutic delivery: a comparison of cationic, PEGylated, and deformable liposomes. Nanotechnology. 2013;24:325101.
16. Fang JY, Hung CF, Hua SC, Hwang TL. Acoustically active perfluorocarbon nanoemulsions as drug delivery carriers for camptothecin: drug release and cytotoxicity against cancer cells. Ultrasonics. 2009;49:39–46.
17. Ruckmani K, Jayakar B, Ghosal SK. Nonionic surfactant vesicles (niosomes) of cytarabine hydrochloride for effective treatment of leukemias: encapsulation, storage, and in vitro release. Drug Dev Ind Pharm. 2000;26:217–22.
18. Hao Y, Zhao F, Li N, Yang Y, Li K. Studies on a high encapsulation of colchicine by a niosome system. Int J Pharm. 2002;244:73–80.
19. Mahale NB, Thakkar PD, Mali RG, Walunj DR, Chaudhari SR. Niosomes: novel sustained release nonionic stable vesicular systems-an overview. Adv Colloid Interf Sci. 2012;183–184:46–54.
20. Selim KMK, Xing ZC, Choi MJ, Chang Y, Guo H, Kang IK. Reduced cytotoxicity of insulin-immobilized CdS quantum dots using PEG as a spacer. Nanoscale Res Lett. 2011;6:528.
21. Edmund AR, Kambalapally S, Wilson TA, Nicolosi RJ. Encapsulation of cadmium selenide quantum dots using a self-assembling nanoemulsion (SANE) reduces their in vitro toxicity. Toxicol In Vitro. 2011;25:185–90.
22. Weng KC, Noble CO, Papahadjopoulos-Sternberg B, Chen FF, Drummond DC, Kirpotin DB, *et al.* Targeted tumor cell internalization and imaging of multifunctional quantum dot-conjugated immunoliposomes in vitro and in vivo. Nano Lett. 2008;8:2851–7.
23. Al-Jamal WT, Al-Jamal KT, Bomans PH, Frederik PM, Kostarelos K. Functionalized-quantum-dot-liposome hybrids as multimodal nanoparticles for cancer. Small. 2008;4:1406–15.
24. Degen JW, Walbridage S, Vortmeyer AO, Oldfield EH, Lonser RR. Safety and efficacy of convection-enhanced delivery of gemcitabine or carboplatin in a malignant glioma model in rats. J Neurosurg. 2003;99:893–8.
25. Generalov R, Kavaliauskiene S, Westrøm S, Chen W, Kristensen S, Juzenas P. Entrapment in phospholipid vesicles quenches photoactivity of quantum dots. Int J Nanomedicine. 2011;6:1875–88.
26. Medintz IL, Uyeda HT, Goldman ER, Mattoussi H. Quantum dot bioconjugates for imaging, labeling and sensing. Nat Mater. 2005;4: 435–46.
27. Li Z, Huang P, Lin J, He R, Liu B, Zhang X, *et al.* Arginine-glycine-aspartic acid-conjugated dendrimer-modified quantum dots for targeting and imaging melanoma. J Nanosci Nanotechnol. 2010;10: 4859–67.
28. Azeem A, Anwer MK, Talegaonkar S. Niosomes in sustained and targeted drug delivery: some recent advances. J Drug Target. 2009;17:671–89.
29. Hou Z, Zhan C, Jiang Q, Hu Q, Li L, Chang D, *et al.* Both FA- and mPEG-conjugated chitosan nanoparticles for targeted cellular uptake and enhanced tumor tissue distribution. Nanoscale Res Lett. 2011;6:563.
30. Chuang KH, Wang HE, Chen FM, Tzou SC, Cheng CM, Chang YC, *et al.* Endocytosis of PEGylated agents enhances cancer imaging and anticancer efficacy. Mol Cancer Ther. 2010;9:1903–12.
31. Cosco D, Paolino D, Muzzalupo R, Celia C, Citrano R, Caponio D, *et al.* Novel PEG-coated niosomes based on bola-surfactant as drug carriers for 5-fluorouracil. Biomed Microdevices. 2009;11:1115–25.
32. Sinnberg T, Lasithiotakis K, Niessner H. Inhibition of PI3K-AKT-mTOR signaling sensitizes melanoma cells to cisplatin and temozolomide. J Investig Dermatol. 2009;129:1500–15.
33. Bafaloukos D, Fountzilas G, Skarlos D, Pavlidis N, Bakoyiannis C, Karvounis N, *et al.* Subcutaneous low doses of interleukin-2 and recombinant interferon alpha with carboplatin and vinblastine in patients with advanced melanoma. Oncology. 1998;55:48–52.
34. Al-Jamal WT, Al-Jamal KT, Tian B, Cakebread A, Halket JM, Kostarelos K. Tumor targeting of functionalized quantum dot-liposome hybrids by intravenous administration. Mol Pharm. 2009;6:520–30.
35. Huang Y, Chen J, Chen X, Gao J, Liang W. PEGylated synthetic surfactant vesicles (niosomes): novel carriers for oligonucleotides. J Mater Sci Mater Med. 2008;19:607–14.
36. Ballou B, Ernst LA, Andreko S, Harper T, Fitzpatrick JA, Waggoner AS, *et al.* Sentinel lymph node imaging using quantum dots in mouse tumor models. Bioconjug Chem. 2007;18:389–96.
37. Greish K. Enhanced permeability and retention (EPR) effect for anticancer nanomedicine drug targeting. Methods Mol Biol. 2010;624:25–37.
38. Biju V, Mundayoor S, Omkumar RV, Anas A, Ishikawa M. Bioconjugated quantum dots for cancer research: present status, prospects and remaining issues. Biotechnol Adv. 2010;28:199–213.
39. Mehta SK, Jindal N. Formulation of tyloxapol niosomes for encapsulation, stabilization and dissolution of anti-tubercular drugs. Colloids Surf B Biointerfaces. 2013;101:434–41.
40. Fernandez-Fernandez A, Manchanda R, McGoron AJ. Theranostic applications of nanomaterials in cancer: drug delivery, image-guided therapy, and multifunctional platforms. Appl Biochem Biotechnol. 2011;165:1628–51.
41. Hsu SH, Wen CJ, Al-Suwayeh SA, Huang YJ, Fang JY. Formulation design and evaluation of quantum dot-loaded nanostructured lipid carriers for integrating bioimaging and anticancer therapy. Nanomedicine. 2013;8:1253–69.